Talanta 115 (2013) 863–869

Contents lists available at SciVerse ScienceDirect

Talanta

journal homepage: www.elsevier.com/locate/talanta

Te oxide nanowires as advanced materials for amperometric nonenzymatic hydrogen peroxide sensing

Maria Rachele Guascito [a,*], Daniela Chirizzi [b], Cosimino Malitesta [a], Tiziana Siciliano [b], Antonio Tepore [b]

[a] Department of Di.S.Te.B.A., University of Salento, Via Monteroni, 73100 Lecce, Italy
[b] Department of Beni Culturali, University of Salento, Via Monteroni, 73100 Lecce, Italy

ARTICLE INFO

Article history:
Received 27 February 2013
Received in revised form
17 June 2013
Accepted 20 June 2013
Available online 5 July 2013

Keywords:
TeO_2 nanowires
Amperometric sensor
Nonenzymatic
H_2O_2 detection

ABSTRACT

A new nonenzymatic platinum Te oxide nanowires modified electrode (Pt/TeO_2-NWs) for amperometric detection of hydrogen peroxide (H_2O_2) is proposed. The modified electrode has been developed by direct drop casting, with TeO_2 nanowires (TeO_2-NWs), synthesized by thermal evaporation of Te(0) in an oxygen atmosphere. The morphological and spectroscopic characterization of the TeO_2-NWs as synthesized on Pt foil was performed by scanning electron microscopy (SEM), X-ray diffraction (XRD) and X-ray photoelectron spectroscopy (XPS) analysis. XPS and XRD analyses are especially involved to gain information on the chemical environment of TeO_2-NWs in contact with Pt surface. Moreover electrochemical characterization of these new modified Pt/TeO_2-NWs modified electrodes was performed by Cyclic Voltammetry (CV) and Cronoamperometry (CA) in phosphate buffer (pH=7; I=0.2) to investigate the sensing properties of this material against H_2O_2. The proposed sensor exhibits a wide linear and dynamic range from 2 μM to 16 mM (R^2=0.9998) and the detection limit is estimated to be 0.6 μM (S/N=3). Moreover, this sensor shows a rapid amperometric response time of less than 5 s and possessed good reproducibility. These results indicate that Pt/TeO_2-NWs composite is suitable to be used as material for sensing applications.

1. Introduction

The analytical determination of hydrogen peroxide is of great practical importance because it is not only the product of the reactions catalyzed by many highly selective oxidases but also an essential component in food, pharmaceutical, environmental and many other fields [1,2]. For H_2O_2 analysis different methods exist such as volumetric, photometry, chemiluminescence, chromatography and electrochemistry. In particular between the electrochemical techniques amperometric determination is among the most used; in fact amperometric nonenzymatic sensors have received considerable interest, because these methods have lower detection limits, short response time and high sensitivity.

Recently nanomaterials have emerged as advanced tools in several research and technology applications because of the possibility of tuning material properties reducing their size [3,4]. This intense interest is due to their unique catalytic, electrocatalytic, electronic, and magnetic properties, which differ greatly from those of the bulk material [5]. Especially nanomaterials with an anisotropic morphology (e.g. tubes and nanowires) are advantageous because they possess a high surface area and multiple contacts (borders, inner and/or outer surfaces) that in principle can be functionalized in several ways [4]. The use of nanomaterials-modified electrodes often exhibit enhanced electrocatalytic performances in terms of activity, sensitivity and stability compared with the respective bare electrodes [5]. Several works based on modified electrodes have been carried out using nanostructured metal oxide (e.g. CuO, ZnO, TiO_2, etc.) to develop electrochemical sensors [6–9]. However the studies relating to the application of new metal oxide nanostructure in electrochemistry are significantly increasing. In this contest the interest towards Te-based (micro-) nanomaterials is often associated to metal Tellurides or Te(0) in different shapes and sizes. In particular, Te (0) microtubes have been applied in sensing applications for hydrogen peroxide [10] and glucose [11]. Only recently, the synthesis of TeO_2 nanowires (NWs) by thermal evaporation of Te (0) in an oxygen atmosphere has been described [12] and one work on structure and characterization of TeO_2 nanoparticles have been reported [13]. TeO_2 is a versatile wide band gap semiconductor material with physical and chemical properties that make it suitable for various technological sensor applications. Conventional processing of TeO_2 material has just been used for preparing

* Corresponding author. Tel.: +39 0832297075; fax: +39 0832297100.
E-mail address: maria.rachele.guascito@unisalento.it (M.R. Guascito).

0039-9140/$ - see front matter © 2013 Elsevier B.V. All rights reserved.
http://dx.doi.org/10.1016/j.talanta.2013.06.032

bulk materials and thin films [14–16]. However, to the best of our knowledge, there were no reports about the development of modified electrode based on Te oxide and applied as electrochemical sensors to detect analytes of biochemical interest in liquid phases.

In this work a new amperometric sensor based on a Pt modified electrode by direct drop casting of the mixture containing TeO_2 nanowires dispersed in ethanol was developed. The spectroscopic characterization of the TeO_2-NWs as synthesized on Pt foil, used as support, was performed by SEM, XRD and XPS analyses. Electrochemical characterization of Pt/TeO_2-NWs electrodes was performed by CV and CA. The collected data evidenced that the presence of TeO_2 nanowires was responsible for an increment of both anodic and cathodic currents in presence of H_2O_2, and promote a remarkable, stable and reproducible response at very low reduction potentials for H_2O_2 of -200 mV vs. SCE in batch analysis.

2. Experimental

Hydrogen peroxide 30%, H_2SO_4, Na_2HPO_4, NaH_2PO_4, TeO_2 powder, and ethyl alcohol, were analytical grade reagents furnished from Sigma. Ultrapure water (Millipore Milli-Q, 18.2 MΩ cm^{-1}) was used. SEM images were taken by using a scanning electron microscope (Tescan Vega/LMU) and XPS analysis was carried out using a Leybold LHS10 spectrometer equipped with an unmonochromatized AlKα source and a SPECS multi-channel detector.

All electrochemical experiments were carried out by using a μStat400 DropSens electrochemical workstation controlled by computer. In batch experiments conventional three-electrode system with a Pt disk (0.0314 cm^2) as working electrode, a Pt wire as counter electrode and a saturated calomel electrode (SCE) as reference were used. All voltammetric and amperometric experiments were carried out in phosphate buffer pH = 7.0 and I = 0.2 (in the text will be indicate as PBS).

The TeO_2-NWs were synthesized by the thermal oxidization of tellurium metal in an oxygen atmosphere flow on platinum foil (1.0 cm^2) following the procedure as reported [13,17]. For electrochemical applications TeO_2-NWs were recovered from Pt foils and transferred in ethanol by sonication.

The surface of Pt electrode was initially polished with alumina, washed and electrochemically pre-treated by CV between -200 mV and +1200 mV in 0.5 M H_2SO_4. Successively the electrode was washed with deionised water and dried with N_2 flow. Modified electrodes were made by casting 20 μL of TeO_2-NWs/ethanol (0.20 mg/200 μL) suspension directly onto Pt electrode surface. Then, the suspension was allowed to evaporate at room temperature. After that Pt/TeO_2-NWs modified electrodes were cycled in PBS starting from measured open circuit potential (OCP), between -200 mV and +800 mV at 10 mV s^{-1} until a steady-state current was obtained (15 voltammetric cycles) to make a stable and reproducible material to be tested as sensor for hydrogen peroxide detection. Then the electrochemical characterization of Pt/TeO_2-NWs modified electrode was performed by cyclic voltammetry between -200 mV and+800 mV vs. SCE in clean PBS at scan rate 50 mV s^{-1}. The modified electrode was washed after preparation and used as amperometric sensor.

3. Results and discussion

3.1. Morphological and spectroscopic characterization

The morphology of as-synthesized TeO_2-NWs was studied by SEM microscopy. In the low magnification image (Fig. 1A) it is visible how nanowires are densely distributed over Pt surface. A single tellurium oxide NW is visible in the high magnification SEM image (Fig. 1B). The XRD spectrum (Fig. 1C) reported here presents several peaks. Asterisk-labeled peaks are ascribed to platinum substrate (JCPDS no.04-0802). The other diffraction peaks are attributed to crystal planes of TeO_2 (JCPDS no.78-1713).

TeO_2-NWs are straight and smooth and their diameters remain nearly constant throughout the length of the wire. Typical diameters range between 300 nm and 850 nm and their lengths can be up to several micrometers.

XPS analysis was carried out on commercial TeO_2 powder as standard and on as-synthesized NWs grown on Pt surface. Fig. 2A and B shows details of high-resolution (HR) spectra of $Te3d_{5/2}$ region that provide binding energy information. The energy scales of the XPS figures reported in this paper are not corrected for surface charging but the peak assignments (Binding Energies, BEs), as reported in the text, are referenced to C1s aliphatic carbon, as an internal standard, set at 285.0 eV [18]. Data analysis and peak de-convolution were performed by means of New Googly software [19] which allows satellites and background correction as well as curve-fitting of photoelectronic peaks. Typically two peak components were used to fit the $Te3d_{5/2}$ HR region for both TeO_2 powder samples and as-synthesized NWs (curves a and b). According to literature data [20], the less intense peak to lower BE (576.7 ± 0.1 eV) recorded for both samples was attributed to Te (IV) oxide. Instead, the peak components to higher BE (579.7 ± 0.1 eV and 579.4 ± 0.1 eV) were tentatively associated to Te mixed oxides of surface [21]. Besides presence of Te(0) is excluded. Also, Pt4f and Te4d HR regions recorded on modified electrode do not show any trace of Pt signal (see supporting S1). This confirms that the surface of TeO_2-NWs is not Pt contaminated. Moreover, as expected, the Te4d component peak was present.

Fig. 2C shows XPS HR spectra of Te $3d_{5/2}$ signal related to Pt/TeO_2-NWs modified electrode after being subjected to almost 10 voltammetric cycles and keep at -300 mV vs. SCE for 550 s until a quasi-zero current was obtained. Typically two peak components were used to fit $Te3d_{5/2}$ region. According to literature [20,22,23] peaks present at 573.7 ± 0.1 and 577.0 ± 0.1 eV (curves a and g), were attributed, respectively, to Te(0) and Te(IV), with a Te(0)/Te (IV) elemental ratio of 0.50 and Te/Pt ratio of 0.52. These data confirm that, the species of tellurium involved in CV experiments, are Te(0) and Te(IV), in the present experimental conditions. In addition no other Te oxidized species are present as expected at pH 7 [24]. In Fig. 2A, B and C the curves c and d represent the "Shirley background" and the X-ray Al anode satellites, respectively. Curves e represent the experimental data (dot curves), while f (solid curves) the overall curve-fitting [25].

3.2. Electrochemical characterization of Pt/TeO_2-NWs

CV was used to study the electrochemical properties of Pt/TeO_2-NWs modified electrode in phosphate buffer pH 7. Fig. 3 shows voltammograms recorded on Pt/TeO_2-NWs (curve b) and on Pt bare as control (curve a), at a sweep rate of 50 mV s^{-1}, respectively, between -600 mV and +800 mV. To better discriminate between Pt bare surface and Pt/TeO_2-NWs modified a difference curve is also reported (curve c).

As expected, Pt bare electrode shows a characteristic cathodic wave, $E_{pc} = -105$ mV, related to the Pt oxide reduction process [26]. Instead in presence of TeO_2-NWs a new well defined anodic wave at E_{pa} = +450 mV is also evident (corrected at +415 mV when obtained using curve difference (c)), while in the reverse scan the cathodic wave was observed at +150 mV (corrected at +170 mV when obtained using curve difference (c)). Chatodic peak is a contribution of both Pt and Te oxide species reduction. According to XPS data, the observed red/ox processes at pH 7 probably

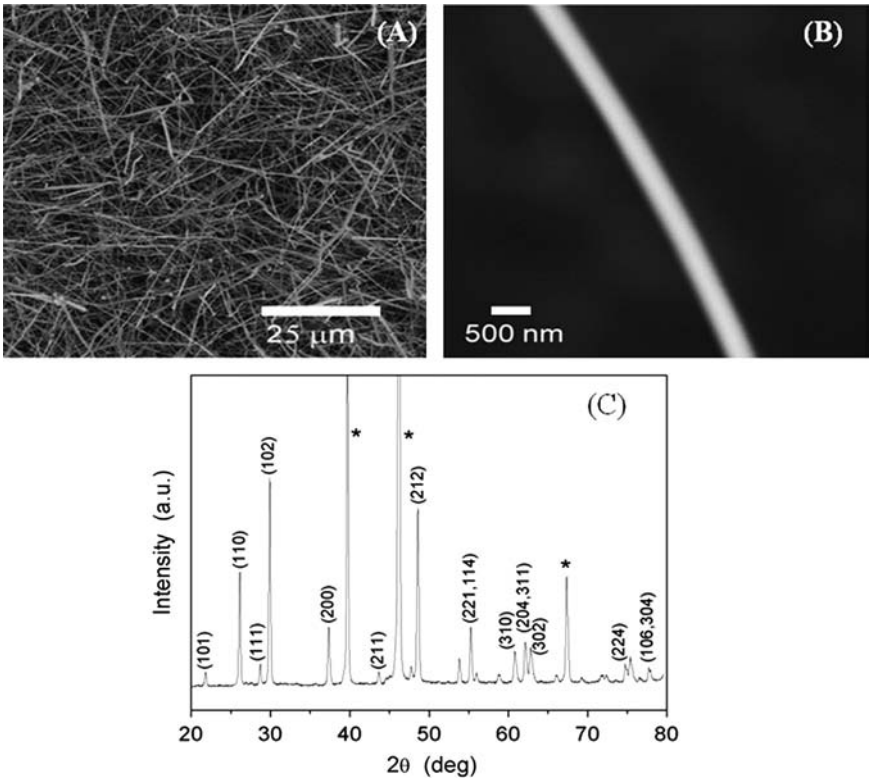

Fig. 1. (A) SEM images of as-synthesized TeO_2-NWs on Pt foil; (B) single TeO_2-NW is visible in the high magnification SEM image; and (C) XRD spectrum of as-synthesized TeO_2-NWs on Pt foil.

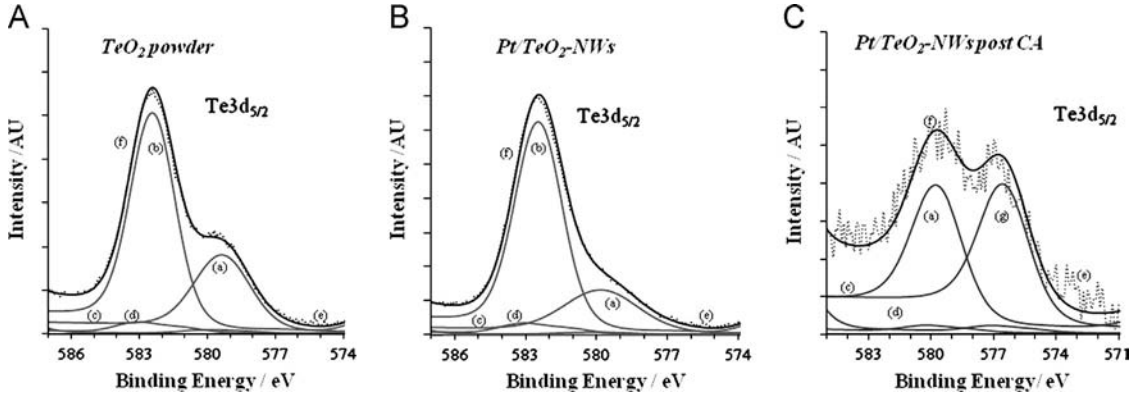

Fig. 2. $Te3d_{5/2}$ detailed spectrum of TeO_2 powder as standard (A), as-synthesized TeO_2-NWs on platinum foil (B) and Pt/TeO_2-NWs after electrochemical treatment (C).

involve the peak pair TeO_2/Te(0) platinum adsorbed species in line with following simplified scheme:

$$Pt/TeO_2+4H^+ + 4e^- \rightarrow Pt/Te+2H_2O \text{ (cathodic overall reaction)} \quad (1)$$

$$Pt/Te+2H_2O \rightarrow Pt/TeO_2+4H^+ + 4e^- \text{ (anodic overall reaction)} \quad (2)$$

This well resolved peak pair (see Fig. 3 curve c) attributed to TeO_2 and Te(0) species is characterized from a calculated formal potential, E_{surf}=+298.0 mV, taken by averaging E_{pa} and E_{pc} at scan rate 5 mV s^{-1}. The measured OCP of +283 mV vs. SCE is shifted to positive potential with respect to Te/TeO_2 powder on Pt confirming that it was more difficult to oxidize Te directly adsorbed on Pt and that the electrochemical behavior of the modified electrode is due to a synergic effect of both species tellurium and platinum [10]. The charge Q involved in oxidation peak measured in steady state condition (50 mV s^{-1}) corrected from the Pt contribution was almost 895 μC cm^{-2}. The charge estimated in oxidation was almost as the charge in reduction ≈760 μC cm^{-2}, as expected from a reaction scheme were the species involved in oxidation process were the same as in the reverse scan. Moreover, adsorbed TeO_2-NWs do not inhibit the adsorption/desorption hydrogen atoms process, as evident in the potential region between −640 and +230 mV (Fig. 3) where instead an increment in currents is observed.

To determine the dynamic characteristics of the electrodic processes, cyclic voltammograms were recorded at different scan rates between 5 and 600 mV s^{-1}, in the potential range between −600 and +800 mV (Fig. 4A). On increasing the scan rate, both the redox peak currents (Fig. 4B) and peak-to-peak separations (Fig. 4C) increased, indicating an irreversible (totally polarized) surface controlled electrode process involving surface confined species [27,28]. In detail, anodic and cathodic peak currents were linearly proportional to the scan rate ranging from 5 and 600 mV s^{-1} (Fig. 4B) with $\alpha \sim 0.5$ obtained from I_{pa} and I_{pc} vs.

slopes.

$$I_{pa}\ (\mu A) = 1.1127\ (\mu A) + 0.0517\ [(\mu A)/(\mathrm{mV/s^{-1}})]v\ (\mathrm{mV/s^{-1}})\quad (R^2 = 0.9908) \tag{3}$$

$$I_{pc}\ (\mu A) = -1.842\ (\mu A) - 0.0556\ [(\mu A)/(\mathrm{mV/s^{-1}})]v\ (\mathrm{mV/s^{-1}})\quad (R^2 = 0.9900) \tag{4}$$

Besides, both the anodic and cathodic potential peaks showed a shift with the increase of the scan rate. Fig. 4C shows the variation of E_{pa} and E_{pc} as a function of Log(v) for TeO_2/Te peak pairs. A linear dependence was evident for both peaks, as expected for a totally irreversible surface process. According to this model, a graph of $E_p = f(\mathrm{Log}\ v)$ yields two straight lines with a slope equal to $2.3RT/\alpha nF$ and intercept $(2.3RT/\alpha nF)\log(\alpha nF/RTks) + E_{surf}$ for the cathodic peak (Eq. (5)). For the anodic peak the slope is $2.3RT/(1-\alpha)nF$ and intercept $[2.3RT/(1-\alpha)nF]\log[(1-\alpha)nF/RTks] + E_{surf}$ (Eq. (6)).

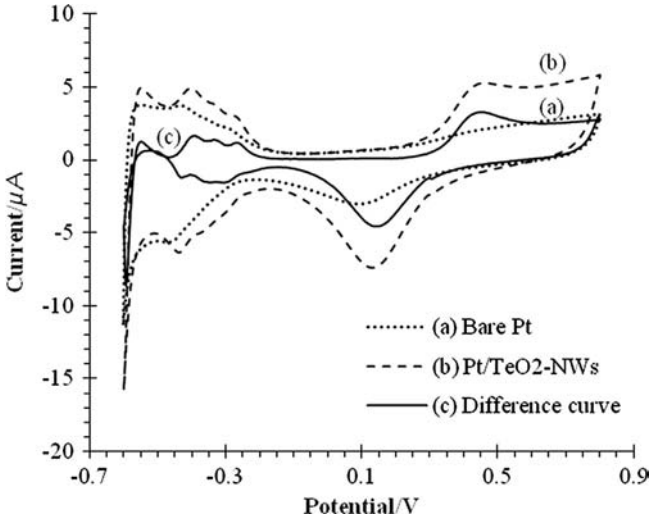

Fig. 3. CV curves recorded in PBS N_2 satured (50 mV s^{-1}) on bare Pt electrode (a) and Pt/TeO_2-NWs modified electrode (b). Curve (c) represents difference voltammogram between curves (a) and (b).

$$E_{pc} - E_{surf} = \left(\frac{-2.3RT}{\alpha nF}\right)\log v - \left(\frac{2.3RT}{\alpha nF}\right)\log\left(\frac{\alpha nF}{RTks}\right) \tag{5}$$

$$E_{pa} - E_{surf} = \left[\frac{2.3RT}{(1-\alpha)nF}\right]\log v + \left[\frac{2.3RT}{(1-\alpha)nF}\right]\log\left[\frac{(1-\alpha)nF}{RTks}\right] \tag{6}$$

From the slopes of the curves (Fig. 4C) values of α and n could be evaluated. α is almost 0.5 (a typical value) and consequently $n=2$ a value lesser than the expected 4 for the overall red–ox processes. These results, suggest that both the overall electrochemical processes ((1) and (2)) occur by more than one slow stage rate determining step [29], were probably also Te (II) species, a product that can disproportionate to form (Te(0) and Te(IV)), is involved [29].

3.3. Electrochemical response to H_2O_2 on Pt/TeO_2-NWs

Cyclic voltammetry was used to study the main electrochemical properties of the Pt/TeO_2-NWs electrode respect to H_2O_2. All experiments were carried out in PBS N_2 saturated a scan rate 50 mV s^{-1}. For comparison, in Fig. 5 voltammograms recorded on bare Pt (orange) and on Pt/TeO_2-NWs (blue) electrodes are reported respectively in the absence and in the presence of H_2O_2 25 μM (Fig. 5A and B). Moreover, Fig. 5C shows responses

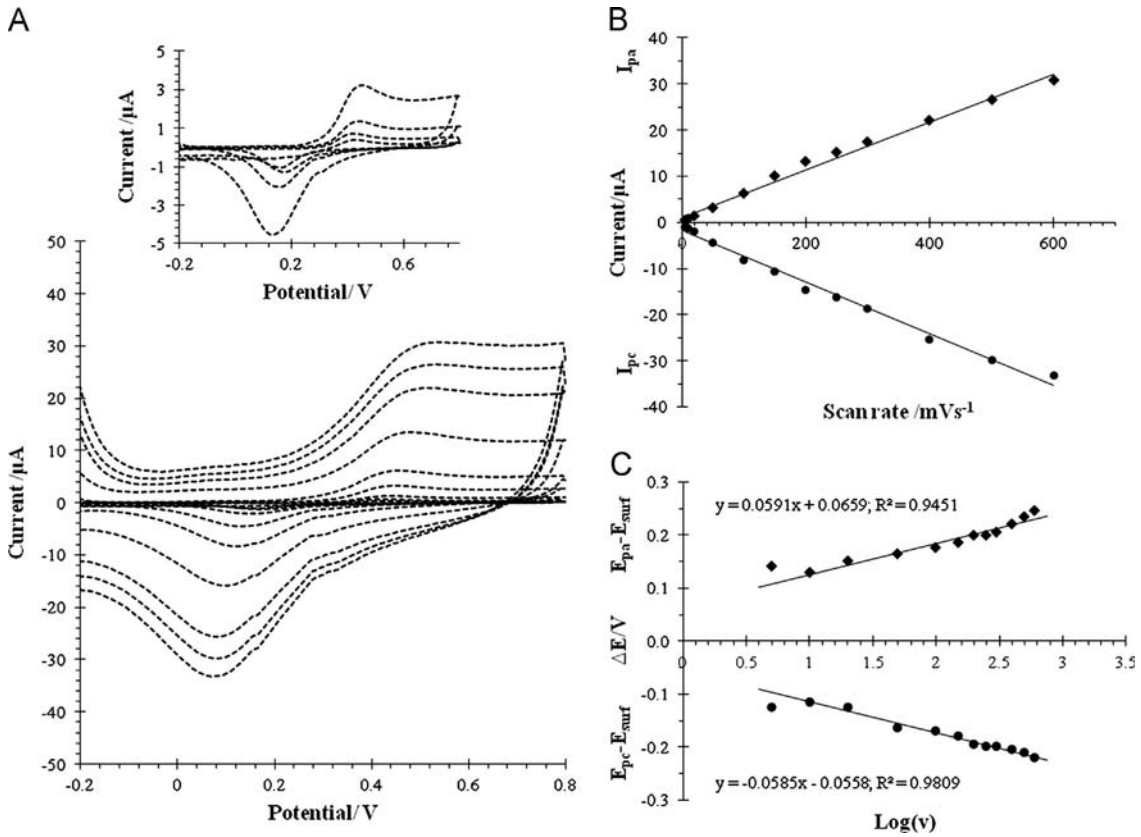

Fig. 4. (A) CV curves recorded on Pt/TeO_2-NWs modified electrode obtained at different scan rate between 5 and 600 mV s^{-1}. (B) Plot of cathodic and anodic peak currents against scan rate. (C) Plot of cathodic (E_{pc}) and anodic (E_{pa}) peak potential against Log(v). Measurement were performed in PBS N_2 satured.

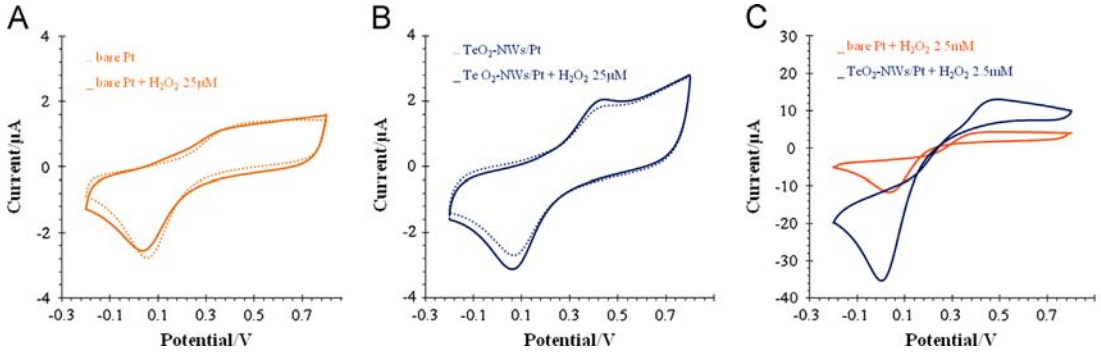

Fig. 5. Cyclic voltammograms recorded in PBS N_2 satured (50 mV s^{-1}): (A) on bare Pt electrode in the absence and in the presence of H_2O_2 25 μM; (B) on Pt/TeO_2-NWs electrode in the absence and in the presence of H_2O_2 25 μM;(C) on bare Pt (orange) and Pt/TeO_2-NWs (blue) electrodes in presence of H_2O_2 2.5 mM. (For interpretation of the references to color in this figure legend, the reader is referred to the web version of this article.)

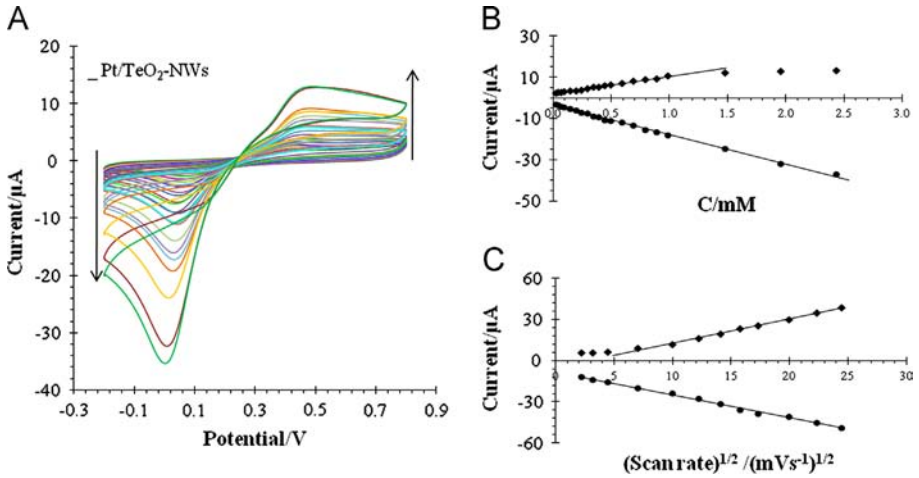

Fig. 6. (A) Cyclic voltammograms recorded in PBS N_2 satured (50 mV s^{-1}) on Pt/TeO_2-NWs electrode to consecutive additions of hydrogen peroxide (0.025–2.5 mM). (B) Plot currents peaks I_{pc} (in reduction) and I_{pa} (in oxidation) against hydrogen peroxide concentration up to 2.5 mM. (C) Plot currents peaks I_{pc} and I_{pa} against the square root of scan rate ν in the interval 5–600 mV s^{-1}. Measurement were performed in PBS N_2 satured.

comparison between Pt/TeO_2-NWs electrode (blue) and bare Pt (orange) for H_2O_2 2.5 mM. Substantial differences were evident between the electrochemical activity recorded on Pt in the presence and in the absence of TeO_2 nanowires.

However, as expected, relevant processes related to H_2O_2 oxidation and reduction was present also on Pt bare electrode. The increment of oxidation current observed on Pt is attributed to H_2O_2 oxidation platinum catalyzed [30]. The corresponding cathodic current increment observed in reduction is related to the reduction of Pt-oxide species and to a process of oxygen reduction generated in oxidation [26]. To tentatively explain the involved processes at Pt/TeO_2-NWs a study of H_2O_2 substrate concentration effect was performed. Fig. 6A shows the response of Pt/TeO_2-NWs electrode to additions of H_2O_2 (concentration range from 25 μM to 2.5 mM).

The catalytic currents I_{pc} in reduction and I_{pa} in oxidation, obtained after subtracting the relative baselines recorded in PBS, were found to increase linearly (Fig. 6B) with H_2O_2 concentration up to 2.5 mM and 1.0 mM respectively, with a determination coefficient of 0.9968 and 0.9954, respectively, deduced by the linear regression analysis carried out with the following (Eq. (7)) in reduction and (Eq. (8)) in oxidation:

$$I_{pc}(\mu A) = -3.526\ (\mu A) - 14.314\ (\mu A\,M^{-1})C\ (mM) \quad (R^2 = 0.9968) \tag{7}$$

$$I_{pa}\ (\mu A) = 1.9379\ (\mu A) + 8.5064(\mu A\,M^{-1})\ C\ (mM) \quad (R^2 = 0.9954) \tag{8}$$

where C is H_2O_2 bulk concentration.

In order to confirm that the electrochemical reduction and oxidation of H_2O_2 are diffusion controlled, it has been estimated the effect of scan rate, on the CV responses. Consistently, at H_2O_2 concentration of 1.0 mM I_{pc} and I_{pa} were found to increase linearly with the square root of scan rate (Fig. 6C) between 50 and 600 mV s^{-1}, with a determination coefficient of 0.9959 and 0.9954 respectively, deduced by regression analysis with the following equations:

$$I_{pc}\ (\mu A) = -1.6687\ (\mu A) - 8.2292\ [\mu A/(mV\ s^{-1})^{1/2}]\nu^{1/2}\ (mV\ s^{-1})^{1/2} \quad (R^2 = 0.9959) \tag{9}$$

$$I_{pa}\ (\mu A) = 1.763\ (\mu A) - 5.0226\ [\mu A/(mV\ s^{-1})^{1/2}]\nu^{1/2}\ (mV\ s^{-1})^{1/2} \quad (R^2 = 0.9954) \tag{10}$$

Based on these results probably in a catalytic simplified reaction scheme (11) in oxidation the H_2O_2 peroxide species reacts with Pt/TeO_2 to regenerate Pt/Te(0) starting material involved in electrochemical oxidation (1). Moreover in reduction (12), the catalytic reaction scheme involves a chemical reaction of H_2O_2 with Pt/Te to regenerate Pt/TeO_2 starting electro-active material (2). In both scheme the rate determining step is the H_2O_2 diffusion at the electrode.

In oxidation: $Pt/TeO_2 + 2H_2O_2 \rightarrow Pt/Te + 2H_2\ O + 2O_2$ (11)

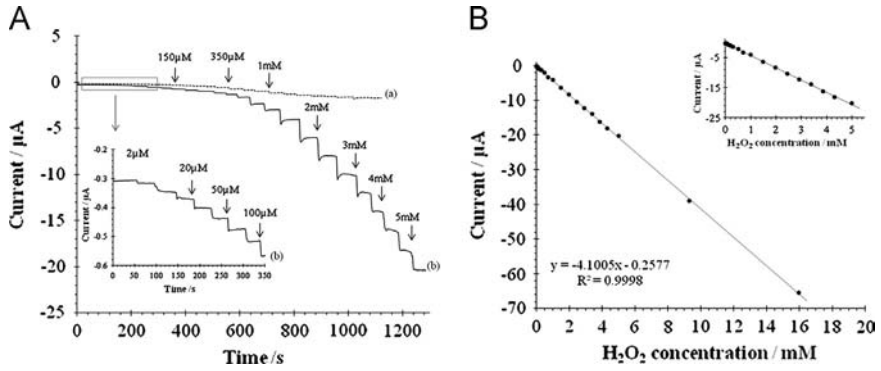

Fig. 7. (A) Amperometric response of Pt/TeO_2-NWs sensor (b) and bare Pt (a) in stirred N_2 satured PBS at an applied potential of −200 mV upon successive addition of H_2O_2. In inset a zoom of the first additions from 2 μM to 100 μM for Pt/TeO_2-NWs sensor. (B) Linear relation between the amperometric response and H_2O_2 concentration. In inset a zoom of calibration curve up to 5 mM.

Table 1
Comparison of various nonenzymatic amperometric H_2O_2 sensors based on nano and micro materials.

Sensor	Sensitivity (μA mM^{-1} cm^{-2})	Liner range (mM)	LOD (μM)	RDS %	Applied potential	PBS (pH)	Ref.
Pt/TeO_2-NWs	130.6	0.002–16	0.6	3.13	−0.2	7.0	[This work]
Fe_3O_4/GC	–	0.0012–3.5	1.2	5.00	−0.5	7.0	[36]
MWCNT/AgNPs	20.10	0.05–17	0.5	3.30	−0.2	7.0	[37]
PVA-MWCNTs-PtNPs	122.63	0.002–8	0.7	3.80	0	7.0	[38]
Se/PtNPs	39.91	0.01–15	3.1	5.00	−0.3	7.0	[39]
PANI/SWCNTs/Pt	–	0.005–1	1.2	–	−0.3	7.0	[40]
Ag/NPs/GC	13.93	0.1–20	1.9	3.9	−0.3	7.4	[41]
Pt/TiO_2/CNT	0.85	0.004–1.25	4	5.5	+0.3	7.4	[9]

NPs: nanoparticelle; CNTs: carbon nanotubes; MWCNTs: multiwall carbon nanotubes; PANI: polyaniline, SWCNTs: single walles carbon nanotubes.

In reduction: $Pt/Te+2H_2O_2 \rightarrow Pt/TeO_2+2H_2O$ (12)

However, most probably the electrocatalytic mechanism of H_2O_2 oxidation and reduction at Pt/TeO_2-NW electrodes, in the present conditions, involves both tellurium and platinum electroactive red–ox pairs in a more complex synergic electrochemical mechanism. As matter of fact both species could be responsible for the catalytic dissociation of H_2O_2 [30–33].

The analytical behavior of Pt/TeO_2-NWs sensor to consecutive additions of H_2O_2 was investigated, at first, by cyclic voltammetry and, then by amperometric detection at a static potential in stirred PBS. The effect of the applied potential was studied on modified electrodes by cronoamperometric measurements, in potentiodynamic conditions, and H_2O_2 1 mM, between −500 mV to +600 mV vs. SCE. The optimal value (−200 mV) was selected as a compromise between the highest current output and the stability of the signal. Typical calibration curves at Pt/TeO_2-NWs sensor and at bare Pt electrode, as control, when hydrogen peroxide was dropped in stirred phosphate buffer (final concentration 16 mM) are reported in Fig. 7A. Though both the electrodes give response to successive H_2O_2 addition, a remarkable increment in registered currents can be observed during experiments involving Pt/TeO_2-NWs sensor. This is a direct evidence of the role played by TeO_2-NWs as promoters of H_2O_2 reduction. Besides on modified electrode the reduction currents increased rapidly to reach a steady-state values within 5 s and Pt/TeO_2-NWs sensor do not seem to suffer of doping effect typically reported on Pt [34]. Moreover the enhanced catalytic activity of Pt/TeO_2-NWs towards the reduction of hydrogen peroxide confirmed the possibility to apply this new material as alternative to be used for biosensor development based on H_2O_2 detection in reduction [35].

Plotting the cathodic current I (μA), measured in each H_2O_2 addition, against its concentrations C (mM), a linear relationship was observed from 2 μM up to 16 mM with a correlation coefficient of 0.9998 (Fig. 7B). Analytical performances of Pt/TeO_2-NWs as sensibility (130.6 μA M^{-1} cm^{-2}), detection limit (estimated to be 0.6 μM at a signal-to-noise ratio of 3) and operating potential (−200 mV vs. SCE) were comparable to recent works based on different conventional electrode modified by nanomaterial for nonenzymatic amperometric hydrogen peroxide sensing (see Table 1). The reproducibility of the sensor was also investigated and the relative standard deviation (RDS%) was 3.13% for the response to H_2O_2 1 mM recorded on three biosensors prepared independently.

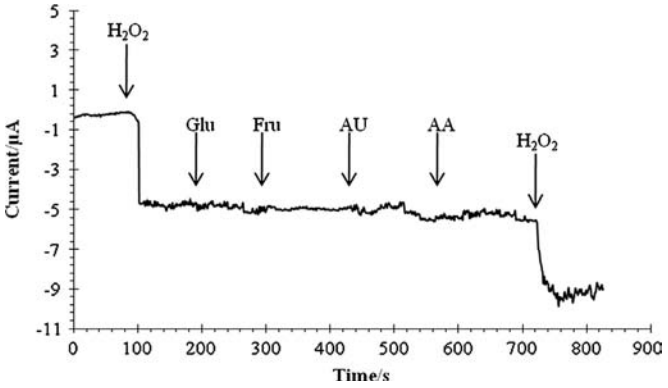

Fig. 8. Amperometric response of Pt/TeO_2-NWs sensor to consecutive injection 1mM of hydrogen peroxide, glucose, fructose, uric acid and ascorbic acid and then again hydrogen peroxide in stirred and nitrogen saturated PBS (pH=7; I=0.2). Applied potential −200 mV vs. SCE.

Sensor selectivity was evaluated by monitoring amperometric response after consecutive injection of 1 mM H_2O_2, 1 mM of each interfering species tested (glucose, fructose, uric acid and ascorbic acid) and again 1 mM H_2O_2. These results were showed in Fig. 8. It was evident that the sensor does not exhibit a significant

response to any of the tested interferences and that the influence of interfering species on response to H_2O_2 was negligible, indicating a high selectivity of the proposed sensor.

4. Conclusions

The main goal of this work is to propose a new nonenzymatic Pt/TeO_2-NWs modified electrode to detect hydrogen peroxide. This is realized by simple Te oxide nanowires spontaneously adsorbed on Pt electrode surface.

Chemical and structural analysis confirms that between Pt and TeO_2 nanowires there are spontaneous and stable interactions. Moreover electrochemical results exhibit remarkable catalytic ability toward hydrogen peroxide reduction with a wide responding range and low detection limit which might be attributed to a synergic effect that involves both Pt and TeO_2 nanowires in enhancing electrocatalitic properties of the new material to hydrogen peroxide reduction. Therefore the electroanalytical Pt/TeO_2-NWs reported performances, along with high selectivity, provides a promising material for the development and application as innovative material for sensing requests.

Acknowledgments

This work was supported by Fondazione Cassa di Risparmio di Puglia (Viale della Repubblica 111, Bari –Italy) regarding the project "*Sviluppo e validazione di metodi basati sull'utilizzo di sensori elettrochimici micro e nano strutturati per la determinazione di analiti di interesse ambiantale in matrici reali*".

Appendix A. Supporting information

Supplementary data associated with this article can be found in the online version at http://dx.doi.org/10.1016/j.talanta.2013.06.032.

References

[1] Y.H. Won, D. Aboagye, H.S. Jang, A. Jitianu, L.A. Stanciua, J. Mater. Chem. 20 (2010) 5030–5034.
[2] E. Nossol, A.J.G. Zarbin, Adv. Funct. Mater. 19 (2009) 3980–3986.
[3] O.D. Velev, S. Gupta, Adv. Mater. 21 (2009) 1897–1905.
[4] G.R. Patzke, F. Krumeich, R. Nesper, Angew. Chem. Int. Ed. (2002)2446–2461.
[5] C.M. Welch, R.G. Compton, Anal. Bioanal. Chem. 384 (2006) 601–619.
[6] A. Umar, M.M. Rahman, Y.B. Hahn, Talanta 77 (2009) 1376–1380.
[7] M.J. Song, S.W. Hwang, D. Whang, Talanta 80 (2010) 1648–1652.
[8] M. Mazloum-Ardakani, H. Rajabi, H. Beitollahi, B.B.F. Mirjalili, A. Akbari, N. Taghavinia, Int. J. Electrochem. Sci. 5 (2010) 147–157.
[9] X. Cui, Z. Li, Y. Yang, W. Zhang, Q. Wang, Electroanalysis 20 (2008) 970–975.
[10] M.R. Guascito, D. Chirizzi, C. Malitesta, E. Mazzotta, M. Siciliano, T. Siciliano, A. Tepore, A. Turco, Biosens. Bioelectron. 26 (2011) 3565–3569.
[11] M.R. Guascito, D. Chirizzi, C. Malitesta, M. Siciliano, T. Siciliano, A. Tepore, Electrochem. Commun. 22 (2012) 45–48.
[12] B. Qin, Y. Bai, Y. Zhou, J. Liu, X. Xie, W. Zheng, Mater. Lett. 63 (2009) 1949–1951.
[13] T Siciliano, A. Tepore, G. Micocci, A. Genga, M. Siciliano, E. Filippo, Sens. Actuators, B—Chem. 138 (2009) 207–213.
[14] A. Vinogradov, V. Lomonov, Y. Pershin, N. Sizova, Cryst. Rep. 47 (2002) 1036–1040.
[15] R. Nayak, V. Gupta, A.L. Dawar, K. Sreenivas, Thin Solid Films 445 (2003) 118–126.
[16] A. Lecomte, F. Bamiere, S. Coste, P. Thomas, J.C. Champarnaud-Mesjard, J. Eur. Ceram. Soc. 27 (2007) 1151–1158.
[17] E. Filippo, G. Micocci, A. Tepore, T. Siciliano, J. Cryst. Growth 336 (2011) 101–105.
[18] National Institute of Standards and Technology—NIST X-Ray Photoelectron Spectroscopy Database Version 3.5, 2003 ⟨http://srdata.nist.gov/xps/⟩.
[19] J.E. Castle, H. Chapman-Kpodo, A. Proctor, A.M. Salvi, J. Electron Spectrosc. 106 (2000) 65–80.
[20] W.P. Zhou, L.A. Kibler, D.M. Kolb, Electrochim. Acta 47 (2002) 4501–4510.
[21] M.H. Patterson, R.H. Williams, J. Phys. D: Appl. Phys. 11 (1978) L83–L86.
[22] G. Hollinger, P. Kumurdjian, J.M. Mackowski, P. Pertosa, L. Porte, T.M. Duc, J. Electron Spectrosc. 5 (1974) 237–245.
[23] C.D. Wagner, L.H. Gale, R.H. Raymond, Anal. Chem. 51 (1979) 466–482.
[24] W. Zhu, J.Y. Yang, X.H. Gao, J. Hou, S.Q. Bao, X.A. Fan, Electrochim. Acta 50 (2005) 5465–5472.
[25] D. Briggs, M.P. Seah, Surface Analysis, second ed., John Wiley & Sons, Inc., New York, 1990.
[26] Y. Gu, C.-C. Chen, Sensors 8 (2008) 8237–8247.
[27] A.J. Bard, L.R. Faulkner, Electrochemical Methods, second ed., Wiley, New York, 2001.
[28] E. Laviron, J. Electroanal. Chem. 101 (1979) 19–28.
[29] A.I. Alekperov, Russ. Chem. Rev. 43 (1974) 235–250.
[30] S.B. Hall, E.A. Khudaish, A.L. Hart, Electrochim. Acta 43 (1998) 579–588.
[31] S.A. Awad, Electrochim. Acta 33 (1968) 925–936.
[32] R. Gerischer, H. Gerischer, Z. Phys. Chem. (N.F) 6 (1956) 178.
[33] J. Weiss, Trans. Faraday Soc. 31 (1935) 1547–1557.
[34] P. Karam, L.I. Halaoui, Anal. Chem. 11 (2008) 5441–5448.
[35] T. You, O. Niwa, M. Tomita, S. Hirono, Anal. Chem. 75 (2003) 2080–2085.
[36] Z. Liu, B. Zhao, Y. Shi, C. Guo, H. Yang, Z. Li, Talanta 81 (2010) 1650–1654.
[37] W. Zhao, H. Wang, X. Qin, X. Wang, Z. Zhao, Z. Miao, L. Chen, M. Shan, Y. Fang, Q. Chen, Talanta 80 (2009) 1029–1033.
[38] Y. Fang, D. Zang, X. Qin, Z. Miao, S Takahashi, J. Anzai, Q. Chen, Electrochim. Acta 70 (2012) 266–271.
[39] Y. Li, J.J. Zhang, J. Xuan, L.-P. Jiang, J.-J. Zhu, Electrochem. Commun. 12 (2010) 777–780.
[40] Q. Wang, Y. Yun, J. Zheng, Microchim. Acta 167 (2009) 153–157.
[41] W. Lu, G. Chang, Y. Luo, F. Liao, X. Sun, J. Mater. Sci. 46 (2011) 5260–5266.